A&A 466, 855–863 (2007)
DOI: 10.1051/0004-6361:20066439

Astronomy & Astrophysics

XMM-Newton broad-band observations of NGC 7582: N_H variations and fading out of the active nucleus

E. Piconcelli[1], S. Bianchi[2,3], M. Guainazzi[2], F. Fiore[1], and M. Chiaberge[4]

[1] Osservatorio Astronomico di Roma (INAF), via Frascati 33, 00040 Monteporzio Catone, Italy
e-mail: piconcelli@oa-roma.inaf.it
[2] European Space Astronomy Center of ESA, Apartado 50727, 28080 Madrid, Spain
[3] Dipartimento di Fisica, Università degli Studi Roma Tre, via della Vasca Navale 84, 00146 Roma, Italy
[4] Space Telescope Science Institute, 3700 San Martin Drive, MD 21218, USA

Received 25 September 2006 / Accepted 7 February 2007

ABSTRACT

We present results from two *XMM–Newton* observations of the bright classical Seyfert 2 galaxy NGC 7582 taken four years apart (2001 May and 2005 April). We present the analysis of the high-resolution (0.3−1 keV) RGS and low-resolution (0.3−10 keV) *EPIC* spectroscopic data. A comparison with a 1998 *BeppoSAX* observation suggests that *XMM–Newton* caught the source in a "reflection-dominated" phase, measuring the lowest continuum flux level ever ($F_{2-10} = 2.3 \times 10^{-12}$ erg cm^{-2} s^{-1}) in 2005. NGC 7582 therefore experienced a dramatic spectral transition most likely due to the partial switching-off of the nuclear activity. The *XMM–Newton* spectrum of the continuum emission is very complex. It can be well described by a model consisting of a combination of a heavily absorbed ($N_H \sim 10^{24}$ cm^{-2}) power law and a pure reflection component both obscured by a column density of $\sim 4 \times 10^{22}$ cm^{-2}. Notably, we detect a significant increase by a factor of ∼2 in the column density of the inner, thicker absorber covering the primary X-ray source between 2001 and 2005. The 2005 *XMM–Newton* spectrum shows the strongest Fe Kα emission line ever measured in this source. This is consistent with the line delayed time response to the decrease of the nuclear activity. Our analysis also reveals that the soft X-ray spectrum is dominated by emission lines from highly ionized metals. The detection of a narrow OVIII radiative recombination continuum suggests an origin in a photoionized plasma.

Key words. galaxies: individual: NGC 7582 – galaxies: active – Galaxy: nucleus – X-ray: galaxies

1. Introduction

In Type 2 Seyfert galaxies the otherwise overwhelming primary continuum emission from the active nucleus is attenuated by the presence of an obscuring screen (the putative dusty torus of the unified model, e.g. Antonucci 1993). This favorable condition enables us to investigate in detail the geometrical and physical properties of the emitting/absorbing gas in the nuclear environment. X-ray observations of obscured sources permit to efficiently map the inner kpc-scale region around the accreting black hole (BH) and understand the physical processes at work in AGN. Recent *XMM–Newton* and *Chandra* results have provided unprecedented insights into the structure and dynamics of the reprocessing materials (see e.g. Risaliti et al. 2005; Iwasawa et al. 2003; Guainazzi & Bianchi 2007, and references therein) and the starburst contribution to the total X-ray emission (e.g. Jimenez-Bailón et al. 2003).

In this paper we present the analysis of two *XMM–Newton* observations of NGC 7582. This source is a highly inclined ($i \sim 65°$) barred spiral galaxy at $z = 0.0053$ (1 arcsec ∼ 110 pc in the source rest-frame). Optical observations reveal a complex morphology, with a kpc-scale disk of H II regions and a prominent dust lane, parallel to the major axis of the galaxy, running across the nuclear region at a distance of some hundreds parsecs (Regan & Mulchaey 1999; Prieto et al. 2002; Wold & Galliano 2006). The optical spectrum is a superposition of a Seyfert 2 nucleus and a starburst (Cid Fernandes et al. 1998; Sosa-Brito et al. 2001). NGC 7582 also shows a sharp-edged [O III] outflow cone (Storchi-Bergmann & Bonatto 1991) having its vertex centered in the (supposedly) hidden nucleus of the host galaxy. All these pieces of evidence suggest that NGC 7582 has a hidden active nucleus lying in a dusty environment and surrounded by circumnuclear starburst.

X-ray observations of NGC 7582 have given further support to this scenario. Thank to its brightness (Piccinotti et al. 1982) this AGN has been targeted by most of the X-ray telescopes: *Einstein* (Maccacaro & Perola 1981), *EXOSAT* (Turner & Pounds 1989), *Ginga* (Warwick et al. 1993), *ASCA* (Schachter et al. 1998; Xue et al. 1998), *BeppoSAX* (Turner et al. 2000, T00 hereafter), and *Chandra* (Bianchi et al. 2007, B07 hereafter). All these studies reported a flat X-ray spectrum dominated by heavy obscuration. The first detailed description of the complex absorber in NGC 7582 was given in T00. Exploiting the unique *BeppoSAX* broad bandpass, these authors reported the detection of two absorbing systems: one fully-covering Compton-thin ($N_H \sim 1.4 \times 10^{23}$ cm^{-2}) screen plus a Compton-thick ($N_H \sim 1.6 \times 10^{24}$ cm^{-2}) absorber covering ∼60% of the X-ray source. Previous X-ray observations of NGC 7582 also revealed rapid short-term (with a factor of ∼2 variations on time scale as short as 5.5 h) as well as complex long-term variability of the hard X-ray flux (e.g. Risaliti et al. 2002).

XMM–Newton observed this source in 2001 for 23 ks and, again, in 2005 for 100 ks. A partial analysis of the first observation, limited to the hard portion (i.e. >2 keV) of the low-resolution *EPIC* spectrum, can be found in Dewangan & Griffiths (2005).

The analysis of the second *XMM–Newton* observation, presented in this paper for the first time, has provided the highest quality X-ray spectrum of NGC 7582 ever obtained. We also reanalyzed the 2001 dataset extending the Dewangan & Griffiths (2005) spectroscopic analysis to the soft X-rays range. For both observations we performed the analysis of the high-resolution (0.3−1 keV) RGS and low-resolution (0.3−10 keV) *EPIC* spectroscopic data.

2. XMM–Newton observations

NGC 7582 was observed by *XMM–Newton* on 2001 May 25 and 2005 April 29 for about 23 and 100 ks, respectively. Both observations were performed with the *EPIC* PN (Struder et al. 2001) and MOS (Turner et al. 2001) cameras operating in full-frame mode.

Data were reduced with SAS 6.5 (Gabriel et al. 2003) using standard procedures. X-ray events corresponding to patterns 0−12(0−4) for the MOS(PN) cameras were selected. The event lists were filtered to ignore periods of high background flaring according to the method presented in Piconcelli et al. (2004) based on the cumulative distribution function of background light curve count-rates. Useful exposure times of 71.2(18.1) ks for the PN and of 81(22.4) ks for the two MOS cameras were obtained for the 2005(2001) observation.

The source photons were extracted from a circular region with a radius of 40 arcsec (32 arcsec in the case of the 2001 observation), while the background counts were estimated from a source-free similar region on the same chip. Appropriate response and ancillary files for all the *EPIC* cameras were created using RMFGEN and ARFGEN tasks in the SAS, respectively. As the difference between the MOS1 and the MOS2 response matrices is a few percent, we created a combined MOS spectrum and response matrix. The background-subtracted spectra for the PN and the combined MOS cameras were then simultaneously fitted. Events outside the 0.3−10 keV range were discarded in the PN spectrum while we restricted the analysis of the MOS data to the 0.5−10 keV range[1].

The RGS (den Herder et al. 2001) was operating in standard spectroscopic mode during the *XMM–Newton* observations. We have therefore reduced also the RGS data using the standard SAS meta-task `rgsproc`, and the most updated calibration files available at the moment the reduction was performed (October 2006). The wavelength systematic uncertainty is 8 mÅ across the whole RGS sensitive bandpass. We refer the reader to Guainazzi & Bianchi (2007) for further details on the data reduction of the RGS dataset.

3. Temporal analysis of the 2005 observation

X-ray light curves were extracted from the 2005 PN dataset in the soft (0.2−2 keV) and hard (2−15 keV) bands. The time bin size was set to be 5000 s for all light curves. Background light curves were extracted from source-free regions in the same CCD and with the same bin size.

The soft X-ray Count Rate (CR) did not vary during the exposure apart a small-amplitude ($\lesssim$20% of the average CR) rapid drop in the bin around $t_{\rm exp} \sim 85$ ks. The hard band light curve did not present any evidence of large-amplitude variability.

The analysis of the hard X-ray variability of the 2001 data has been recently presented by Awaki et al. (2006). They reported a smooth and nearly linear decrease ($\lesssim$30%) of the hard X-ray CR from the start up to the end of the observation, which is confirmed by our analysis. In addition, we have also extracted the soft X-ray band light curve for this observation. The 0.2−2 keV CR remained almost steady during the exposure with only a decrease of approximately 2σ from the average CR level in the final interval.

4. Spectral analysis

All spectra were analyzed with the XSPEC v11.2 package (Arnaud 1996). All models discussed in this paper include absorption due to the line-of-sight Galactic column of $N_{\rm H} = 1.47 \times 10^{20}$ cm^{-2} (Stark et al. 1992). The cosmology assumed has $H_0 = 70$ km s^{-1} Mpc^{-1}, $\Omega_{\rm m} = 0.3$, and $\Omega_\Lambda = 0.7$ (Bennett et al. 2003). The quoted errors on the model parameters correspond to a 90% confidence level for one interesting parameter ($\Delta\chi^2 = 2.71$; Avni 1976).

4.1. The hard X-ray continuum

Given the spectral complexity of NGC 7582, we began our analysis by fitting the *EPIC* data in the 3−10 keV range.

We initially assumed the "dual absorber" model used by T00 for the 3−100 keV *BeppoSAX* data consisting of a power law modified by two neutral absorbers, one of which (the thicker) only partially covers the primary X-ray source. We also included two narrow Gaussian lines in order to account for the iron Kα and Kβ emission features, which were both clearly visible in the spectrum. The energy of the Kβ line was fixed to 7.06 keV. In the case of the 2005 spectrum we also added in the model two narrow Gaussian lines at 6.67 and 7.55 keV to reproduce the FeXXV Kα and NiXXI Kα emission. Each line represents an improvement in the resulting fit statistics significant at 99.9% confidence level.

This parameterization ($dual_{3-10}$ hereafter) provided a very good fit to both *XMM–Newton* datasets with a final χ^2_ν(d.o.f.) = 0.96(204) and χ^2_ν(d.o.f.) = 0.94(172) for the 2005 and 2001 observations, respectively (Table 1). The continuum slope and the column density of the fully-covering absorber did not differ between the two epochs. On the contrary, the 2005 spectrum shows a much stronger Fe Kα line with an $EW \sim 700$ eV. We also found a significant change in the best-fit value of the column density of the partially-covering absorbing screen with an increase of $\Delta(N_{\rm H}^{\rm p}) \sim 25 \times 10^{22}$ cm^{-2}, while the covering factor remained unchanged ($C_{\rm f} = 90\%$)

We then adopted a model consisting of an absorbed power law plus an unabsorbed pure Compton reflection component from neutral matter (`PEXRAV` model in XSPEC, e.g. Magdziarz & Zdziarski 1995, with the metal abundances fixed to the solar value, the inclination angle fixed to 65 deg) reflecting a power-law with the same photon index of the absorbed primary continuum. Such a model has been found to successfully reproduce the X-ray spectrum of most heavily-obscured Seyfert 2 galaxies observed by *XMM–Newton* so far (e.g. Schurch et al. 2002; Matt et al. 2004; Bianchi et al. 2005a). Narrow Gaussian lines were included as in the $dual_{3-10}$ model. This model (indicated as $refl_{3-10}$ hereafter) gave an equally good description of the hard X-ray spectrum of NGC 7582 with an associated χ^2_ν(d.o.f.) = 0.93(205) (χ^2_ν(d.o.f.) = 0.96(173) for the 2001

[1] In the case of the lower statistics data from the 2001 observation, we ignored the MOS data below 1 keV due to the presence of cross-calibration uncertainties between the MOS cameras in the 0.3−1 keV band which could prevent an unbiased determination of the PN+MOS best-fit spectral model (Stuhlinger et al. 2006).

Table 1. Spectral fitting results for the $dual_{3-10}$ model applied to the hard (3−10 keV) band. For comparison the results obtained using the 1998 *BeppoSAX* data are also listed (e.g. Sect. 5).

	Γ	$N_{\rm H}{}^a$ 10^{22} cm^{-2}	$N_{\rm H}{}^b$ 10^{22} cm^{-2}	$C_{\rm f}{}^c$ %	EW(Fe Kα)^d eV	$F_{3-10}{}^e$ 10^{-12} erg cm^{-2} s^{-1}
XMM-Newton 2005	$2.35^{+0.19}_{-0.19}$	$9.4^{+1.0}_{-0.8}$	$93.5^{+6.7}_{-3.2}$	90	715^{+365}_{-101}	1.1
XMM-Newton 2001	$2.28^{+0.27}_{-0.27}$	$10.2^{+2.7}_{-3.4}$	$66.9^{+8.3}_{-4.4}$	90	330^{+70}_{-40}	1.7
BeppoSAX 1998	$2.06^{+0.08}_{-0.14}$	$16.9^{+1.5}_{-1.5}$	$265.1^{+115.5}_{-64.1}$	50	83^{+23}_{-29}	11.7

^{a} "Fully-covering" absorber. ^{b} "Partially-covering" absorber. ^{c} Best-fit covering factor. ^{d} Measured for an absorption-corrected line against absorption-corrected continuum. ^{e} An absorbed power-law model with $\Gamma = 1.7$ and $N_{\rm H} = 1.5 \times 10^{22}$ cm^{-2} was assumed.

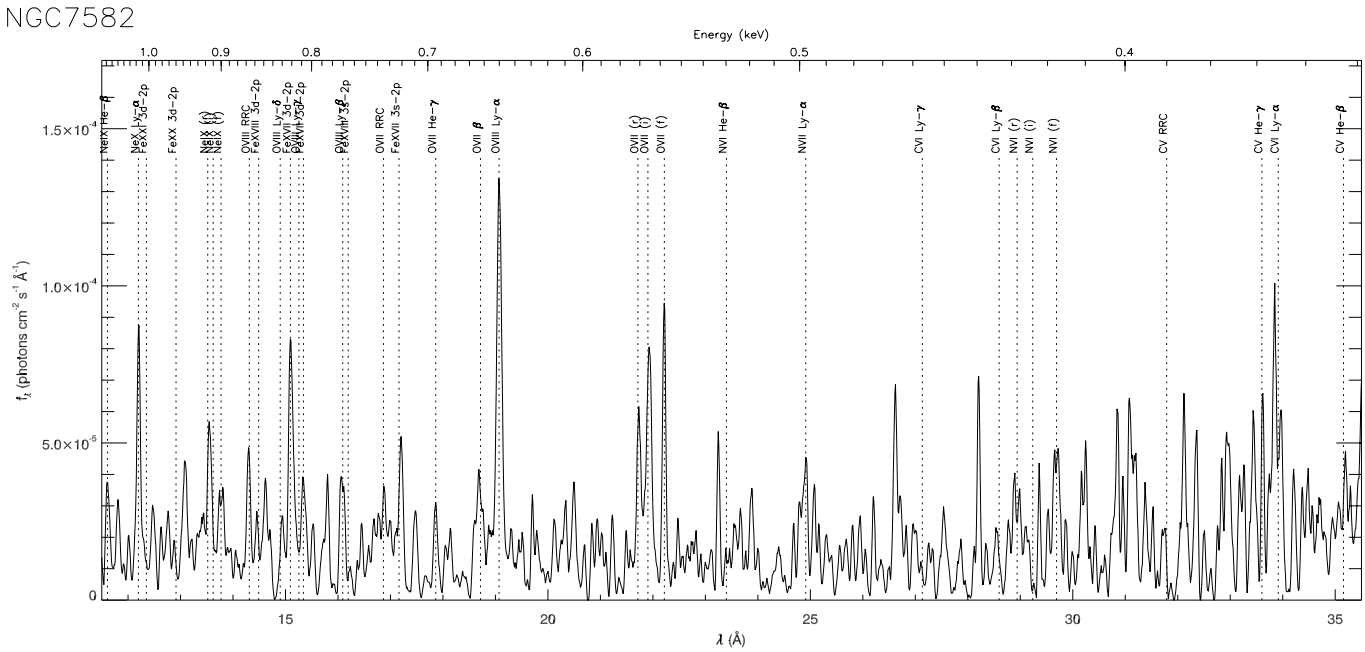

Fig. 1. RGS *fluxed* spectrum of NGC 7582 resulting from the merging of the 2005 and 2001 *XMM–Newton* observations. The positions of the main emission lines produced in a photoionized plasma are labeled. The emission lines significantly detected in the spectrum of each single RGS camera are only those listed in Table 2 (see Sect. 4.2 for details).

data). For the 2005 spectrum we measured a $\Gamma = 2.40^{+0.18}_{-0.20}$ and a column density of $N_{\rm H} = (140^{+16}_{-13}) \times 10^{22}$ cm^{-2}. The energy centroid (EW) of the Fe Kα line was 6.404±0.006 (802^{+49}_{-45} eV, calculated with respect to the pure reflection component). This energy corresponds to low ionization states, i.e. FeI–XIII (Kallman et al. 2004).

The application of the $refl_{3-10}$ model to the 2001 hard X-ray spectrum yielded results consistent with those reported by Dewangan & Griffiths (2005), i.e. $\Gamma = 2.08^{+0.29}_{-0.29}$ and $N_{\rm H} = (75^{+9}_{-9}) \times 10^{22}$ cm^{-2}. This fit gave, therefore, a further confirmation for an increase in the level of absorption between 2001 and 2005. On the contrary, the values of the normalization of the reflection component and the intensity of the Fe Kα line are consistent with being the same in the two *XMM–Newton* observations within errors. This fact is not surprising since both these spectral features are believed to be the result of reprocessing of the primary (obscured) X-ray emission in a distant material ($\gtrsim$1 pc from the X-ray source).

Models $dual_{3-10}$ and $refl_{3-10}$ are statistically indistinguishable. However, they correspond to very different physical scenarios for the hard X-ray emission in NGC 7582, requiring either the presence of two different absorbers ("transmission scenario") or reflection/reprocessing from optically thick matter ("reflection-dominated scenario"), respectively. We extensively discuss both scenarios and their implications in Sect. 5 and in Sect. 6.1.

4.2. The 0.3–10 keV spectrum

The extrapolation of the hard X-ray models (see Sect. 4.1) to energies lower than 3 keV shows the presence of a smooth continuum excess along with several narrow excess features. This excess has been observed in most of X-ray obscured Seyfert galaxies (Turner et al. 1997) and, thanks to *Chandra* and *XMM–Newton* high-resolution spectroscopy, it has been interpreted as a combination of reflected emission of the hidden nuclear continuum by a warm gas (and/or a tiny leaked fraction of the nuclear emission) with unresolved blends of emission lines, which originate from the same gas (e.g. Sako et al. 2000; Sambruna et al. 2001; Matt et al. 2004; Pounds & Vaughan 2006; Bianchi et al. 2005a; B07).

The analysis of the RGS spectrum lends support to this interpretation, revealing for the first time that the soft X-ray emission of NGC 7582 is clearly dominated by emission lines, as shown in Fig. 1. This figure is generated by combining the 1st

Table 2. List of the emission lines (plus OVIII RRC) detected in the RGS data and those included in the *EPIC* best fit model along with their likely identification.

Line Id. (Å)	RGS data		EPIC data	
	λ (Å)	Intensity (10^{-5} ph/cm^2/s)	λ (Å)	Intensity (10^{-5} ph/cm^2/s)
CVI Ly-α(33.74)	33.78(33.73, 33.83)	1.07(0.22, 1.86)		
NVII Ly-α(24.78)	24.80(24.70, 24.84)	0.68(0.28, 1.11)		
OVII He-$\alpha(f)$(22.10)	22.10*	1.37(0.87, 1.88)	22.10†	1.33(1.15, 1.58)
OVII He-$\alpha(i)$(21.80)	21.80*	0.87(0.40, 1.39)		
OVII He-$\alpha(r)$(21.60)	21.60(21.59, 21.61)	0.97(0.48, 1.50)		
OVIII Ly-α(18.97)	18.98(18.97, 18.99)	1.47(1.13, 1.85)	18.97†	0.97(0.84, 1.14)
OVII He-β(18.63)	18.66(18.62, 18.69)	0.22(0.06, 0.55)		
FeXVII 3s2p(17.08)	17.10(17.08, 17.11)	0.69(0.48, 1.07)		
FeXVIII 3s2p(16.09)	16.03(15.99, 16.08)	0.45(0.21, 0.67)	16.09†	0.78(0.67, 0.92)
OVIII Ly-β(16.00)	16.02(15.98, 16.10)	0.29(0.11, 0.53)		
FeXVII 3d2p^{3}D$_1$(15.26)	15.26†	0.96(0.73, 1.32)		
FeXVII 3d2p^{1}P$_1$(15.01)	15.01(15.00, 15.03)	1.07(0.80, 1.43)	14.79(14.77, 14.88)	1.97(1.78, 2.04)
FeXVIII 3d2p(14.41)	14.51(14.48, 14.55)	0.32(0.09, 0.60)		
NeIX He-α(r)(13.45)	13.48(13.46, 13.52)	0.86(0.36, 1.37)	13.45†	1.62(1.55, 1.79)
OVIII RRC(14.22)	14.22†	0.30(0.11, 0.71)		
FeXXI 3d2p(12.28)	12.15(12.11, 12.19)	0.54(0.13, 0.97)	12.21(12.16, 12.26)	1.30(1.15, 1.35)
FeXXIV 3d2p(11.18)			11.18†	0.41(0.34, 0.47)
NeX Ly-β(10.24)			10.35(10.26, 10.45)	0.29(0.21, 0.33)
MgXI He-α(9.23)			9.21(8.99, 9.24)	0.46(0.38, 0.49)
MgXII Ly-α(8.42)			8.53(8.43, 8.59)	0.14(0.11, 0.22)
MgXII Ly-β(7.10)			7.10†	0.09(0.06, 0.13)
SiXIV Ly-α(6.18)			6.18(6.15, 6.23)	0.19(0.12, 0.22)
SiXIII He-α(6.69)			6.68(6.66, 6.71)	0.48(0.43, 0.56)
SXV He-α(5.04)			5.07(5.05, 5.09)	0.32(0.26, 0.36)
SXVI Ly-α(4.72)			4.68(4.60, 4.76)	0.05(0.02, 0.11)
FeXXV Kα(1.86)			1.86†	0.23(0.15, 0.31)
Fe Kβ(1.76)			1.76†	0.32(0.24, 0.40)
NiXXI Kα(1.64)			1.65(1.63, 1.66)	0.17(0.10, 0.25)

The values in parentheses in Cols. 2 to 5 indicate the minimum and the maximum limits of the 90% confidence interval for each parameter. * The wavelength of the forbidden f and the intercombination i lines were fixed to be at +0.5 and +0.2 Å from the resonance line best-fit wavelength; † fixed value.

and 2nd order spectra of the two RGS cameras, and smoothing the combined spectra through a convolution with a 5-spectral channel wide triangular function. Errors are not shown in the *fluxed* spectrum of Fig. 1, which is presented for illustration purposes only since the applied smoothing procedure can amplify any spurious features due to instrumental issues as, for instance, in the case of the two strong unidentified emission lines visible at 26.5 and 28.3 Å that correspond to chip gaps in RGS2 CCD array (and are not associated with any relevant atomic transition). Table 2 reports the parameters of the lines detected by a combined forward-folding fit of the spectra of the two RGS cameras, employing the spectral fitting procedure outlined in Guainazzi & Bianchi (2007). Their origin and the implications concerning the physical properties of the emitting gas are discussed in detail in Sect. 6.2.

For the above reasons, we added a power-law component to the *refl*$_{3-10}$ model to account for the continuum "soft excess" emission. The photon index was constrained to be that of the primary (absorbed) continuum but the normalization was left free to vary. For the reasons explained in the Sect. 6, model *refl*$_{3-10}$ turns out to be physically preferable to model *dual*$_{3-10}$ and we therefore used the former as baseline model for the broad band *EPIC* spectrum of NGC 7582. Apart from the strongest emission lines detected in the RGS spectrum in the range 0.3−1 keV, we also included in the fitting model eight narrow Gaussian lines, required at a significance level of >99%, to account for the strongest emission features observed in the ∼1−3 keV band, where the RGS detectors are less sensitive. Table 2 lists the best-fit parameters together with the likely identification for each of these lines as measured in the longest observation. Finally, no absorption line is required by the data.

This extension of the model *refl*$_{3-10}$ to the broad band produced a $\chi^2(\nu) \gtrsim 1.2$ for both *XMM–Newton* datasets[2], indicating that such a parametrization of the continuum spectral shape was not satisfactory. However, a very significant (≫99.9% confidence level) improvement was obtained by including in this fit an additional absorber obscuring both the primary emission and the Compton reflection. We derived column densities of $N_{\rm H} = (3.9^{+0.5}_{-0.7}) \times 10^{22}$ cm^{-2} (2001 value), and $N_{\rm H} = (4.8^{+0.4}_{-0.6}) \times 10^{22}$ cm^{-2} (2005 value). On the contrary, as already pointed out in Sect. 4.1, the column density of the inner, thicker absorber covering only the primary continuum increased by a factor of about 2.4 ($\Delta N_{\rm H} \approx 7 \times 10^{23}$ cm^{-2}) between 2001 and 2005. The best-fit parameters yielded by the application of this model (*refl* hereafter) are listed in Table 3. Spectral residuals and unfolded spectral models are shown in Figs. 2 and 3.

[2] Given the high complexity of the broad band spectrum and the poorer statistics of the 20 ks spectrum taken in 2001, we constrained the value of the normalization of the reflection component to vary within the 99% confidence level interval derived for the same parameter from the 2005 data. The 2001 and 2005 unconstrained values for this parameter were consistent within errors.

Table 3. Spectral fitting results for the model *refl* applied to the broad (0.3−10 keV) band.

Obs. (1)	Γ (2)	$N_{\rm H}$ (3)	$A_{\rm pl}^{\rm cont}$ (4)	$A_{\rm pl}^{\rm scatt}$ (5)	I(Fe Kα) (6)	EW(Fe Kα) (7)	Flux (8)	Lum. (9)	χ^2(d.o.f.) (10)
2005	$1.93^{+0.01}_{-0.01}$	$4.8^{+0.4}_{-0.6}$ [a]	35^{+3}_{-3}	$1.06^{+0.02}_{-0.02}$	23^{+1}_{-1}	772^{+46}_{-36} [c]	3.8[d]	41.68[d]	381(361)
		$129.3^{+5.5}_{-6.7}$ [b]					23.5[e]	41.86[e]	
2001	$1.90^{+0.05}_{-0.02}$	$3.9^{+0.5}_{-0.7}$ [a]	35^{+2}_{-5}	$1.06^{+0.04}_{-0.03}$	22^{+2}_{-3}	620^{+66}_{-79} [c]	3.7[d]	41.68[d]	295(272)
		$54.9^{+6.6}_{-2.1}$ [b]					40.2[e]	41.89[e]	

The columns give the following information: (1) the observation date; (2) the power-law photon index; (3) the absorber column density of the absorber (10^{22} cm^{-2}); (4) the normalization of the absorbed power law (10^{-4} photons/keV/cm^2/s); (5) the normalization of the scattered power law (10^{-4} photons/keV/cm^2/s); (6) the intensity of the Fe Kα line (10^{-6} photons/cm^2/s); (7) the Fe Kα equivalent width (eV); (8) the flux (10^{-13} erg cm^{-2} s^{-1}); (9) the logarithmic value of luminosity (erg/s); (10) the reduced χ^2 and the number of degrees of freedom. [a] Absorber covering the reflected component and the primary continuum. [b] Absorber covering only the primary continuum. [c] Measured with respect to the pure reflection component. [d] Value for the 0.5−2 keV band. [e] Value for the 2−10 keV band.

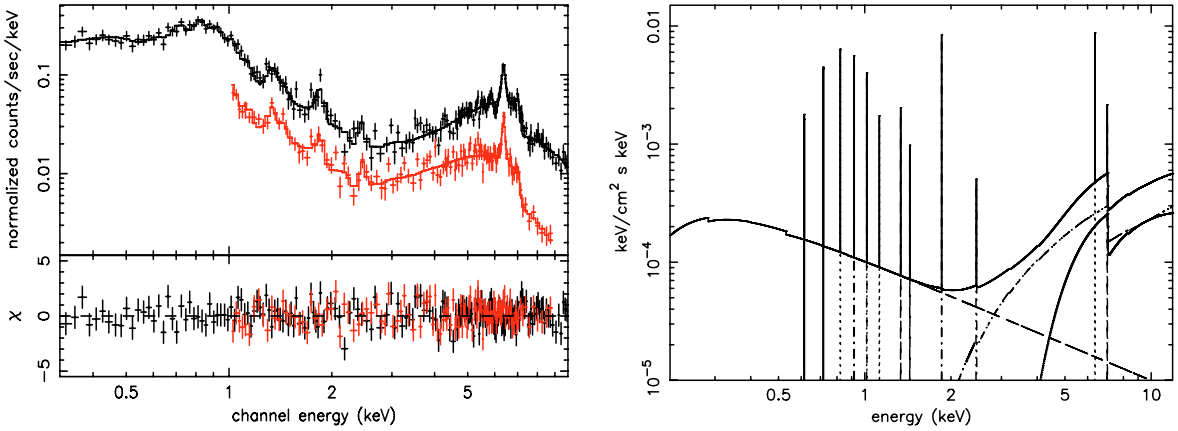

Fig. 2. *Left*: 2001 *XMM–Newton* PN (*top*) and MOS (*bottom*) spectra of NGC 7582 when the *refl* model is applied. The lower panel shows the deviations of the observed data from the model in unit of standard deviations. *Right*: best-fit model for the reflection-dominated scenario. This model consists of an absorbed ($N_{\rm H} \sim 6 \times 10^{23}$ cm^{-2}) power law, a pure reflection component (both obscured by a column density of $\sim 4 \times 10^{22}$ cm^{-2}) plus an additional unobscured power law component accounting for the soft X-ray scattered/leaked emission. It also includes twelve narrow Gaussian emission lines.

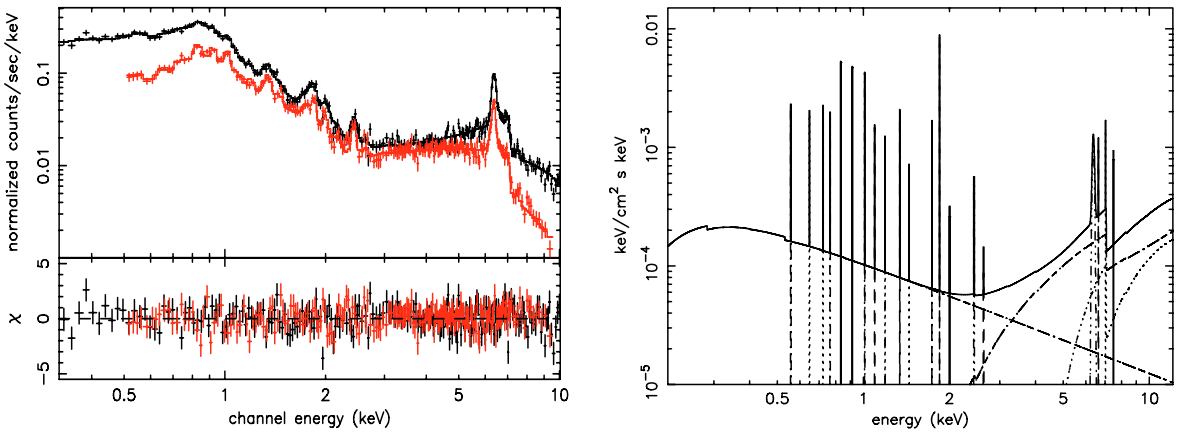

Fig. 3. *Left*: 2005 *XMM–Newton* PN (*top*) and MOS (*bottom*) spectra of NGC 7582 when the *refl* model is applied. The lower panel shows the deviations of the observed data from the model in unit of standard deviations. *Right*: best-fit model (*refl*) for the 2005 *EPIC* spectrum. See Tables 2 and 3 for further details.

5. *XMM–Newton* versus *BeppoSAX* results: evidence of a spectral transition

In Fig. 4a the 2001 3–10 keV PN spectrum and the 3–90 keV *MECS+PDS* spectra are plotted together and fitted by the best-fit model used by T00 for the continuum emission above 3 keV (which is similar to our *dual*$_{3-10}$ model). It is worth noting the decrease of the X-ray flux between the two epochs: *XMM–Newton* caught, in fact, the source in a extremely faint state with a 3−10(8−10) keV flux lower than a factor of ∼7(4) if compared with the *BeppoSAX* observation. NGC 7582 was even fainter during the second *XMM–Newton* observation performed four years later as shown in Fig. 4b. Among the previous studies of NGC 7582, the *XMM–Newton* continuum flux levels (e.g. $F_{2-10}^{2001} = 4 \times 10^{-12}$ erg cm^{-2} s^{-1} and $F_{2-10}^{2005} = 2.3 \times 10^{-12}$ erg cm^{-2} s^{-1}) are the lowest ever

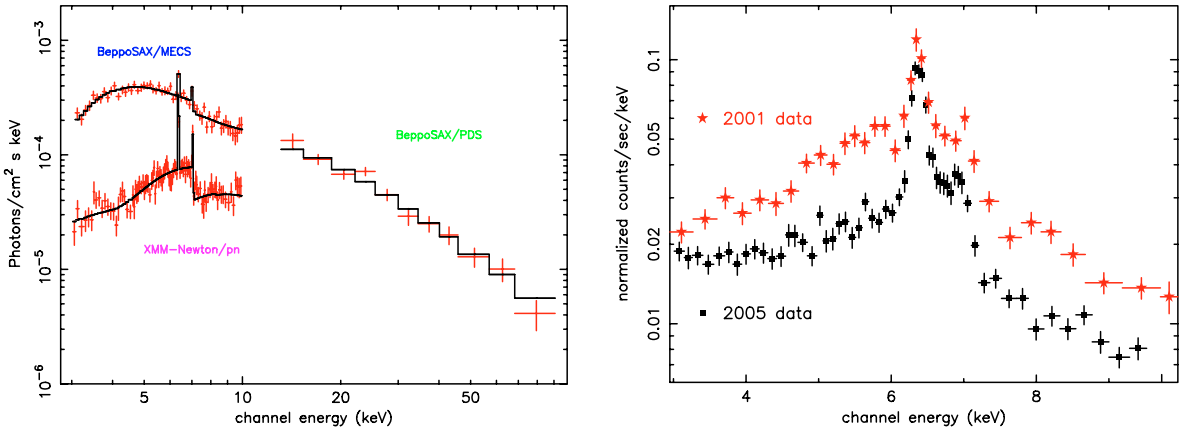

Fig. 4. a) *Left*: unfolded 1998 *BeppoSAX* (MECS and PDS) and 2001 *XMM–Newton* PN spectra of NGC 7582 fitted by the dual$_{3-10}$ model (e.g. Sect. 5 for details). This figure clearly shows the large variations in the spectral shape and intensity occurred in the source between the two observations. **b)** *Right*: 3−10 keV PN data from the observations of 2001 May and 2005 April. This plot demonstrates the progressive decline of the hard X-ray flux.

measured: *EXOSAT* ($F_{2-10} \sim 1.7 \times 10^{-11}$ erg cm^{-2} s^{-1}, Turner & Pounds 1989), *ASCA* ($F_{2-10} \sim 1.5 \times 10^{-11}$ erg cm^{-2} s^{-1}, Xue et al. 1998) and *Ginga* ($F_{2-10} \sim 6 \times 10^{-12}$ erg cm^{-2} s^{-1}, Warwick et al. 1993) all observed the source in a brighter state.

Spectral variations are also evident between the *BeppoSAX* and *XMM–Newton* observations (see Table 1 and Fig. 4). The *XMM–Newton* spectrum of NGC 7582 shows the typical features (i.e. a strong iron line emerging from a hard and curved continuum) of a source in a "reflection-dominated" phase. The detection of a prominent Fe Kα line (*EW* ∼ 700 eV; see Table 1) coupled with the excellent fit to the data provided by the model *refl*$_{3-10}$ (e.g. Sect. 4.1) suggest that the X-ray emission detected by *XMM–Newton* can be considered as the echo of primary – i.e. nuclear – continuum during a prior phase of more intense nuclear activity. This change of appearance from a transmission- to reflection-dominated spectral state (or vice versa, e.g. Guainazzi et al. 2002) was reported by Matt et al. (2003) and Bianchi et al. (2005b) in a handful of Seyfert 2 galaxies. They argued that this temporal behavior can be due to switching-off (or following re-emergence) of the nuclear activity.

6. Discussion

6.1. A possible geometry for the nuclear region in NGC 7582

In this section we focus on the properties of the very complex X-ray spectrum above ∼3 keV with the aim of providing a physically acceptable scenario for the nuclear emission of NGC 7582.

Both the *refl*$_{3-10}$ and the *dual*$_{3-10}$ model describe the data equally well (see Sect. 4.1). However, the comparison between the *BeppoSAX* and *XMM-Newton* X-ray spectra leads us to favor the former on the basis of physical considerations. In a pure transmission-dominated scenario with the 2005(2001) X-ray continuum attenuated by a column of $N_{\rm H} \sim 9(7) \times 10^{23}$ cm^{-2} there is no explanation for the presence of a strong Fe Kα line with an *EW* of ∼700 (330) eV (e.g. Matt 2002). It is also worth noting that during the *XMM–Newton* exposures of NGC 7582 no rapid and large-scale variations in the hard band light curve occurred, at odds with previous *ASCA* and *BeppoSAX* observations which caught the source in a clear transmission-dominated phase. This suggests that the primary X-ray source has experienced a large-amplitude decline prior to the 2001 *XMM–Newton* observation unmasking the reflection component underlying the primary emission. Hereafter we therefore refer to the reflection-dominated spectral state model (i.e. *refl*) as the most physically acceptable description of the *XMM–Newton* broad band spectra of NGC 7582.

A similar apparent switching-off of the nucleus was observed in other Seyfert 2 galaxies (e.g. Guainazzi et al. 2005b, G05 hereafter) and even in Type 1 AGN (Guainazzi et al. 1998). The physical reason of this phenomenon is likely associated with variations in the accretion flow onto the BH (Uttley et al. 1999) or, at least in some cases, with dramatic changes in the properties (i.e. column density, covering factor) of the line-of-sight absorber (e.g. Risaliti et al. 2005; Elvis et al. 2004; Matt et al. 2003). It is worthwhile to notice that in NGC 7582 the AGN continuum has not completely disappeared as a significant component of transmitted (absorbed) nuclear emission is detected (e.g. Figs. 2, 3 and Table 3).

Our best-fit model for both *XMM–Newton* observations requires the presence of two absorbers (e.g. Table 3): a screen with $N_{\rm H} \approx 4 \times 10^{22}$ cm^{-2}, which blocks both primary and reflected emission, and a medium with $N_{\rm H} \approx 5-10 \times 10^{23}$ cm^{-2} which obscures the nuclear source only. In the following we will refer to them as the thin and the thick absorber, respectively.

The gas responsible for the reflection is most likely located at the far inner side of the molecular *torus* (i.e. the cylindrically-symmetric compact dusty absorber invoked in the simplest version of the AGN unified models, e.g. Krolik & Begelman 1988; Antonucci 1993; see also Jaffe et al. 2004). Given the column density of the thick absorber, it is quite straightforward to associate it to the *torus*. This in turn implies that the thin absorber surrounds both the central engine and reflecting/reprocessing region and, therefore, should be located well beyond the pc-scale distance usually attributed to the *torus*. A sketch of the proposed absorption geometry in the circumnuclear region of NGC 7582 is shown in Fig. 5.

This scenario is also supported by the discovery of an increase of a factor of ∼2.4 in the column density of the thick absorber between the two *XMM–Newton* observations (i.e. over an interval of about 4 yr). Interestingly, similar large-amplitude variations of the absorbing column over the whole X-ray history of NGC 7582 were reported by Risaliti et al. (2002). They measured a fast variation in the $N_{\rm H}$ value by a factor of 1.2 in a time interval of six months. The $N_{\rm H}$ change observed between the

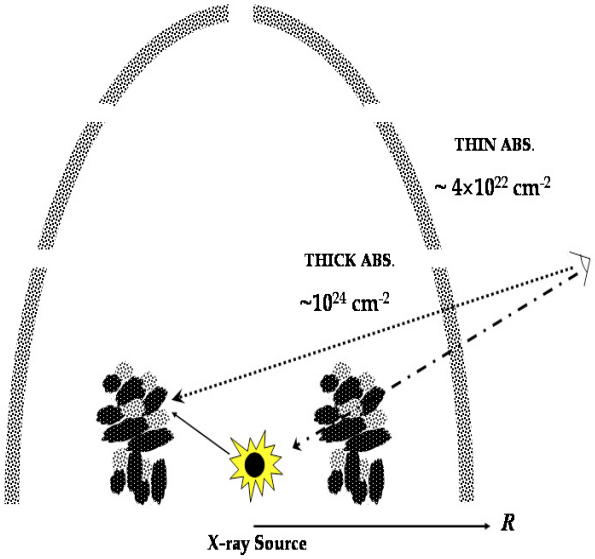

Fig. 5. Sketch of the absorption geometry in the circumnuclear region of NGC 7582 according to model *refl*. The *dotted* and *dotted-dashed* lines represent the X-ray lines of sight. A fraction of the X-ray continuum intercepts (*solid line*) the inner surface of the thick ($N_{\rm H} \sim 10^{24}$ cm^{-2}) absorber and is reflected via Compton scattering along our line of sight. These photons scattered in our direction will then pass through the large-scale thin absorber, which is located far away from the central X-ray source, and be absorbed by a column density of $N_{\rm H} \sim 4 \times 10^{22}$ cm^{-2}. This figure is not to scale.

XMM–Newton observations is, however, one of the largest amplitude detected so far. As suggested by Risaliti et al. (2002) and Matt et al. (2003), these variations cast serious doubts on the existence of a single homogeneous absorber (i.e. *torus*) as invoked in the simplest version of the unified models for AGN. They instead support a more complex scenario whereby the obscuring gas is largely inhomogeneous in space or time, with multiple absorbing components distributed in a range of distances from fractions of parsec up to several hundreds parsecs from the central supermassive BH.

Our results also corroborate the conclusions drawn by B07 on the basis of *Chandra* and *HST* images of NGC 7582. The extremely high value of the nuclear flux ratio between 1.6 and 0.6 μm measured for this Seyfert galaxy suggests, in fact, the presence of a second intervening absorber more external than the expected *torus*. This could be linked to a prominent dust lane and/or dusty compact regions associated with starburst formation (e.g. Sosa-Brito et al. 2001; Wold & Galliano 2006) in this source. The *XMM–Newton* observations presented in this paper provide us with the direct evidence of the existence of two circumnuclear absorbing regions and allow us to shed light on their location.

This finding also agrees with the results presented by Guainazzi et al. (2005b) on the basis of a large sample of Seyfert 2 galaxies observed with *Chandra* or *XMM–Newton* and *HST* high-resolution optical coverage. They found that the presence of dust lane is correlated with values of the X-ray column density in the Compton-thin range. Even if the large-scale dust lanes seen in *HST* images do not seem to be directly responsible for the X-ray obscuration, these authors suggested that a dusty inner host galaxy environment may favor the formation of clumps/filaments of X-ray Compton-thin absorbing matter with large covering fractions.

These results lend support to the model presented by Matt (2000). He proposed a modification of the simplest version of the unification model for AGN whereby the line of sight of Compton-thick Seyfert 2 galaxies intercepts a compact distribution of dense matter (the *torus*) close ($\lesssim$1−10 pc) to the nucleus, while Compton-thin Seyfert galaxies are viewed through absorbing patches likely associated with the dust lane(s) extending on scales of hundreds of parsecs observed in all Seyfert galaxies (see Malkan et al. 1988; Maiolino & Rieke 1995). As predicted by this model, in the case of NGC 7582 our line of sight intercepts both the *torus* and the "Compton-thin" regions which, therefore, coexist in this source.

6.1.1. The Fe Kα emission line

The *EW* values of the Fe Kα line at 6.4 keV derived from the *XMM–Newton* observations, i.e. $EW^{2001} \sim 330$ and $EW^{2005} \sim 700$ eV assuming a transmission-dominated scenario (see Table 1), are by far the largest measured in NGC 7582 so far. All previous X-ray observations reported a weaker feature with an $EW \lesssim 150$ eV. However, when calculated with respect to the reflection component, the 2001 value of the line *EW* of ∼600 eV (e.g. Table 3) appears to be relatively low if compared with the expected one, i.e ∼1 keV (Matt et al. 1996), and usually observed in reflection-dominated sources (G05). Nonetheless, an iron K line with a $EW \sim 600$ eV has been recently detected in the mildly Compton-thick Seyfert galaxy Mrk 3 by Bianchi et al. (2005a). They suggested to explain such an Fe Kα line intensity by the combination of iron under-abundance and a small inclination angle (i.e. $\ll$90 deg) between our line of sight and the symmetry axis of reflecting medium. This interpretation might hold also for NGC 7582.

However, it is also worth noting that nearly all the reflection-dominated sources observed to date are truly Compton-thick, i.e. obscured by a $N_{\rm H} \gtrsim \sigma_t^{-1} \approx 1.6 \times 10^{24}$ cm^{-2}, while the 2001 *XMM–Newton* spectrum of NGC 7582 turns out to be absorbed by a smaller column density (i.e. $N_{\rm H} \sim 5.5 \times 10^{23}$ cm^{-2}). Furthermore, in most of the theoretical calculations the geometry of the reflector is assumed to be a parallel slab illuminated by an isotropic X-ray source and this assumption may be incorrect in the case of NGC 7582. In fact, as emerged from this paper, the properties of the nuclear region in this Seyfert galaxy seems to be peculiar, with a lot of (variable) components contributing to the complex observed spectrum.

6.2. The soft X-ray emission

The combination of *EPIC*+RGS data provides by far the best quality spectrum of the soft X-ray emission in NGC 7582 to date. Our spectral analysis of these data has revealed that this emission is dominated by a wealth of emission lines from different ions (Fig. 1) superimposed on a very faint (i.e. $\lesssim$2% of the primary continuum) scattered continuum.

Table 2 shows the most prominent emission lines detected both in the RGS and in the *EPIC* spectra. All the line widths are unresolved and most of them were identified with hydrogen- and helium-like lines of the most abundant metals, from carbon to sulfur. The strongest lines are associated to the OVII He-α and OVIII Ly-α transitions. An intense OVIII Ly-α is usually found in galaxies with powerful starburst activity (e.g. Guainazzi & Bianchi 2007). However, B07 found no spatial correlation between the peaks of the OVIII emission and the optical star-forming regions in the high-resolution composite *Chandra* and

HST image of NGC 7582. Furthermore, the detection of the narrow OVIII Radiative Recombination Continuum (RRC) can be interpreted as strong evidence for recombination in a low-temperature photoionized plasma. In fact, in a collisional plasma these features are broad and weak and, therefore, hardly discernible above the bremsstrahlung continuum (Liedahl 1999). The presence of Fe L (i.e. FeXVII-XVIII) features can also provide further information on the nature of the line-emitting gas. The larger intensity of the 3d–2p lines with respect to the 3s–2p ones is at odds with the expectations for a recombination-dominated plasma, suggesting an important contribution from photoexcitation of bound-bound transitions by the continuum radiation field (Kallman et al. 1996; Sako et al. 2000).

This discovery significantly improves our understanding of the nature of the "soft excess" emission in this Seyfert galaxy. In fact, previous *ASCA* and *BeppoSAX* observations did not provide firm conclusions on the origin of this spectral component. T00 invoked the presence of emission from a collisionally ionized gas (`mekal` model in XSPEC), accounting for 41% of the total 0.1−2 keV flux, plus a "leaking" unabsorbed fraction (∼0.4%) of the hard X-ray continuum power law. Xue et al. (1998) suggested a mixture of scattered and thermal emission without detecting any emission line due to the poor statistics of their *ASCA* data.

A detailed discussion on the soft X-ray emission morphology of NGC 7582 has been presented in B07 on the basis of high-resolution *Chandra* and *HST* images. According to B07, the hard X-ray *Chandra* image is dominated by the nuclear unresolved emission while the soft X-ray emission is extended over ∼20 arcsec. The large-scale dust lane visible in the optical image strongly affects the morphology of this soft X-ray emission. In particular, most of it arises on the west side of the nucleus where the dust lane is optically thinner and, remarkably, exhibits similarity with the [O III] radiation cone-shaped structure detected by Storchi-Bergmann & Bonatto (1991).

BO6 also present evidence for two "hot spots" i.e. regions where emission from higher ionization stages of O and Ne is enhanced. These "hot-spots" appear to be unrelated with nuclear star-forming regions, and therefore suggest that the star-forming activity does not provide an important contribution to the ionization of the soft X-ray emitting gas. Such a conclusion can be also inferred by our analysis. The far infrared (FIR) luminosity of NGC 7582 is $L_{\rm FIR} \sim 9.6 \times 10^{43}$ erg s^{-1} (Taniguchi & Ohyama 1998). Using the relationship between FIR and soft X-ray luminosity discovered by Ranalli et al. (2003) on a large sample of star-forming galaxies, we estimate a starburst contribution $\lesssim$5% to the total soft X-ray luminosity in NGC 7582 (i.e. $L_{0.5-2} = 4.8 \times 10^{41}$ erg s^{-1}).

7. Summary

We have presented the spectral analysis of the *EPIC*+RGS data from two *XMM–Newton* observations of the bright Seyfert 2 galaxy NGC 7582 (May 2001 and April 2005). The main results from our analysis can be summarized as follows:

- The spectrum of the broadband continuum emission is very complex. It can be well described by a model consisting of a combination of a heavily absorbed ($N_{\rm H} \sim 12.9(5.5) \times 10^{23}$ cm^{-2} in the 2005(2001) spectrum) power law and a pure reflection component, both obscured by an additional absorber with column density of $\sim 4 \times 10^{22}$ cm^{-2}.
  We consider this model as the most physically plausible description for the *XMM–Newton* data on the basis of the following observational pieces of evidence. Firstly, the hard X-rays light curves do not show any rapid and/or large amplitude variation which are typically observed in "transmission-dominated" Seyfert 2 galaxies and, in particular, in all previous observations of NGC 7582. Noteworthy, the 2−10 keV flux level during both *XMM–Newton* observations (i.e. $F^{2005}_{2-10}(F^{2001}_{2-10}) \sim 2(4) \times 10^{-12}$ erg cm^{-2} s^{-1}) are by far the lowest values measured for this source to date. Secondly, comparing the *XMM–Newton* spectra with that obtained from a 1998 *BeppoSAX* observation (see Fig. 4), it appears evident that NGC 7582 experienced a dramatic spectral transition. The most prominent spectral feature above 3 keV is the strong narrow Fe Kα line at 6.4 keV ($EW^{2005} \sim$ 700 eV). All these pieces of evidence lend support to a scenario according to which *XMM–Newton* caught the source in a Compton reflection-dominated phase with a very faint level of the (absorbed) primary continuum and a strong reflection component.
- Our best-fit model requires the presence of two absorbers, with the thinner (i.e. $N_{\rm H} \sim 4 \times 10^{22}$ cm^{-2}) one obscuring both primary and reflected emission. This finding further strengthens the conclusions reported by Guainazzi et al. (2005a) and Matt et al. (2003) about a distribution of the X-ray absorbing gas much more complex than that usually assumed in the most popular Unified models for AGN. In particular, the X-ray spectrum of NGC 7582 confirms the presence of a multiplicity of absorbing regions coexisting in the same source. We have detected an unprecedented increase in the column density of the inner, thicker absorber of $\Delta N_{\rm H} \sim 7.4 \times 10^{23}$ cm^{-2} between 2001 and 2005, while, on the contrary, the $N_{\rm H}$ of the second absorber remained unchanged. This huge variation suggests strong clumpiness and inhomogeneity of the absorbing matter along the line of sight. A likely explanation for the observed spectral variability is the drift of clouds located very near the central source as proposed by Risaliti et al. (2005) and Lamer et al. (2003) to account for similar changes in the obscuring column density of NGC 1365 and NGC 3227, respectively.
  Future observations above 10 keV of NGC 7582 will be crucial to shed light on the properties of the X-ray continuum emission as well as the geometry and variability pattern of the obscuring gas in the nuclear environment of this peculiar Seyfert 2 galaxy.
- The analysis of the high resolution RGS spectrum has revealed that soft X-ray excess in this obscured AGN is dominated by a wealth of emission lines with a very low level of scattered/leaked continuum. According to the recent *Chandra* results presented by B07, this emission is extended on a hundreds-pc scale and, remarkably, its shape and location are very similar to the optical [OIII] ionization cone observed by Storchi-Bergmann & Bonatto (1991). The most prominent emission lines originate from H- and He-like ions of O, C and Ne as well as by L-shell transitions of FeXVII. The detection of a narrow OVIII RRC strongly suggests that most of the soft X-ray emission arises in a photoionized plasma. These findings are in agreement with the few high-resolution soft X-ray spectroscopic measurements published to date (e.g. Sambruna et al. 2001; Young et al. 2001; Kinkhabwala et al. 2002; Guainazzi & Bianchi 2007).

Acknowledgements. We would like to thank the staff of the *XMM–Newton* Science Operations Center for their support. Useful discussions with Fabrizio Nicastro are acknowledged. This research has made use of the NASA/IPAC Extragalactic Database (NED) which is operated by the Jet Propulsion Laboratory, California Institute of Technology, under contract with the National Aeronautics and Space Administration. E.P. acknowledges the financial support from INAF.

References

Antonucci, R. 1993, ARA&A, 31, 473
Arnaud, K. A. 1996, ASP Conf. Ser, 101, 17
Awaki, H., Murakami, H., Ogawa, Y., & Leighly, K. M. 2006, ApJ, 645, 928
Bennett, C. L., Halpern, M., Hinshaw, G., et al. 2003, ApJS, 148, 1
Bianchi, S., Miniutti, G., Fabian, A. C., & Iwasawa, K. 2005a, MNRAS, 360, 380
Bianchi, S., Guainazzi, M., Matt, G., et al. 2005b, A&A, 442, 185
Bianchi, S., Guainazzi, M., & Chiaberge, M. 2006, A&A, 448, 499
Bianchi, S., Chiaberge, M., Piconcelli, E., & Guainazzi, M. 2007, 374, 697 (B07)
Cid Fernandes, R., Storchi-Bergmann, T., & Schmitt, H. R. 1998, MNRAS, 297, 579
den Herder, J. W., Brinkman, A. C., Kahn, S. M., et al. 2001, A&A, 365, L7
Dewangan, G. C., & Griffiths, R. E. 2005, ApJ, 625, L31
Elvis, M., Risaliti, G., Nicastro, F., et al. 2004, ApJ, 615, L25
Gabriel, C., Denby, M., Fyfe, D. J., Hoar, J., & Ibarra, A. 2003, in Astronomical Data Analysis Software and Systems XIII, ed. F. Ochsenbein, M. Allen, & D. Egret (San Francisco: ASP), ASP Conf. Ser., 314, 759
Gu, M. F., Kahn, S. M., Savin, D. W., et al. 1999, ApJ, 518, 1002
Guainazzi, M., & Bianchi, S. 2007, MNRAS, 374, 1290
Guainazzi, M., Nicastro, F., Fiore, F., et al. 1998, MNRAS, 301, L1
Guainazzi, M., Matt, G., Fiore, F., & Perola, G. C. 2002, A&A, 388, 787
Guainazzi, M., Matt, G., & Perola, G. C. 2005a, A&A, 444, 119
Guainazzi, M., Fabian, A. C., Iwasawa, K., et al. 2005b, MNRAS, 356, 295 (G05)
Jaffe, W., Meisenheimer, K., Röttgering, H. J. A., et al. 2004, Nature, 429, 47
Jimenez-Bailon, E., et al. 2003, ApJ, 593, 127
Kallman, T. R., Liedahl, D., Osterheld, A., Goldstein, W., & Kahn, S. 1996, ApJ, 465, 994
Kallman, T. R., Palmeri, P., Bautista, M. A., Mendoza, C., & Krolik, J. H. 2004, ApJS, 155, 675
Kinkhabwala, A., Sako, M., Behar, E., et al. 2002, ApJ, 575, 732
Krolik, J. H., & Begelman, M. C. 1988, ApJ, 329, 702
Lamer, G., Uttley, P., & McHardy, I. M. 2003, MNRAS, 342, L41
Liedahl, D. A. 1999, in X-Ray Spectrocopy in Astrophysics, ed. J. van Paradijs, & J. A. M. Bleeker (Berlin: Springer), 189
Maccacaro, T., & Perola, G. C. 1981, ApJ, 246, L11
Magdziarz, P., & Zdziarski, A. 1995, MNRAS, 273, 837
Maiolino, R., & Rieke, G. H. 1995, ApJ, 454, 95
Makishima, K. 1986, Lecture Notes Phys., 266, 246
Malkan, M. A., Gorjian, V., & Tam, T. 1998, ApJS, 117, 25
Matt, G. 2000, A&A, 355, L31
Matt, G. 2002, MNRAS, 337, 147
Matt, G., Brandt, W. N., & Fabian, A. C. 1996, MNRAS, 280, 823
Matt, G., Guainazzi, M., & Maiolino, R. 2003, MNRAS, 342, 422
Matt, G., Bianchi, S., D'Ammando, F., & Martocchia, A. 2004, A&A, 421, 473
Molendi, S., Bianchi, S., & Matt, G. 2003, MNRAS, 343, L1
Piccinotti, G., Mushotzky, R. F., Boldt, E. A., et al. 1982, ApJ, 253, 485
Piconcelli, E., Jimenez-Bailon, E., Guainazzi, M., et al. 2004, MNRAS, 351, 161
Pounds, K., & Vaughan, S. 2006, MNRAS, 368, 707
Prieto, M. A., Reunanen, J., & Kotilainen, J. K. 2002, ApJ, 571, L7
Ranalli, P., Comastri, A., & Setti, G. 2003, A&A, 399, 39
Regan, M. W., & Mulchaey, J. S. 1999, AJ, 117, 2676
Risaliti, G., Elvis, M., & Nicastro, F. 2002, ApJ, 571, 234
Risaliti, G., Elvis, M., Fabbiano, G., Baldi, A., & Zezas, A. 2005, ApJ, 623, L93
Sako, M., Kahn, S. M., Paerels, F., & Liedahl, D. A. 2000, ApJ, 543, L115
Sambruna, R. M., Netzer, H., Kaspi, S., et al. 2001, ApJ, 546, L13
Schachter, J. F., Fiore, F., Elvis, M., et al. 1998, ApJ, 503, L123
Schurch, N. J., Roberts, T. P., & Warwick, R. S. 2002, MNRAS, 335, 241
Sosa-Brito, R. M., Tacconi-Garman, L. E., Lehnert, M. D., & Gallimore, J. 2001, ApJS, 136, 61
Stark, A. A., Gammie, C. F., Wilson, R. W., et al. 1992, ApJS, 79, 77
Storchi-Bergmann, T., & Bonatto, C. J. 1991, MNRAS, 250, 138
Struder, L., Briel, U., Dennerl, K., et al. 2001, A&A, 365, L18
Stuhlinger, M., et al. 2006, XMM-SOC-CAL-TN-0052, Issue 3.0 [arXiv:astro-ph/0511395]
Taniguchi, Y., & Ohyama, Y. 1998, ApJ, 507, L121
Turner, T. J., & Pounds, K. A. 1989, MNRAS, 240, 833
Turner, T. J., George, I. M., Nandra, K., & Mushotzky, R. F. 1997, ApJS, 113, 23
Turner, T. J., Perola, G. C., Fiore, F., et al. 2000, ApJ, 531, 245 (T00)
Turner, M. J. L., Abbey, A., Arnaud, M., et al. 2001, A&A, 365, L27
Uttley, P., McHardy, I. M., Papdakis, I. E., Guainazzi, M., & Fruscione, A. 1999, MNRAS, L6
Ward, M. J., Wilson, A. S., Penston, M. V., et al. 1978, ApJ, 223, 788
Warwick, R. S., Sembay, S., Yaqoob, T., et al. 1993, MNRAS, 265, 412
Wold, M., & Galliano, E. 2006, MNRAS, 369, L47
Xue, S., Otani, C., Mihara, T., Cappi, M., & Matsuoka, M. 1998, PASJ, 50, 519
Young, A. J., Wilson, A. S., & Shopbell, P. L. 2001, ApJ, 556, 6